ENSO-Induced Variability in Vertical Mixing in the Central Equatorial Pacific

Cody Cruz

University of Washington

School of Oceanography

Seattle WA 98105

openonic@uw.edu

3/8/2024

Data, code, and documentation is available at https://github.com/GHOpenonic/equatorial pacific-turbulent-mixing

Abstract

The El Niño Southern Oscillation (ENSO) sets an important global atmospheric state for climate and weather, impacting agriculture, population health, and other sectors. Evaluating the factors that influence El Niño and La Niña conditions is invaluable for predicting them. Vertical mixing is one important positive feedback in sea surface temperature (SST), responsible for the oscillations of ENSO. During an El Niño, as trade wind velocity decreases, Equatorial Undercurrent (EUC) velocity decreases, reducing subsurface shear and mixing, which increases SST, reducing wind velocity further. Mixing can be parametrized with such metrics as Richardson numbers R_i, Thorpe Scales L_T, and turbulent dissipation rates ε. Data to evaluate these metrics were obtained with Acoustic Doppler Current Profilers (ADCP) and Conductivity, Temperature, and Depth (CTD) profiles from warming La Niña and peak warming El Niño cruises without Tropical Instability Wave (TIW) presence, demonstrating the 'background state' of mixing. The integrated probability density of normalized R_i distributions associated with high mixing potentials from EUC-induced shear was 0.33 for La Niña 2023 and 0.17 for El Niño 2024. These results demonstrate increased mixing potential during La Niña. There is also the possibility of fast density-inversion smoothing (no large L_T) both years. These 'background state' results were qualitatively compared with three studies utilizing TAO data, ARGO float data, and a numerical model with general agreement. Various approaches to the ENSO equatorial vertical mixing problem yielded consistent results across different time and distance scales, important to understanding the broader impacts of ENSO on mixing and climate.

Plain Language Summary

When the surface of the Equatorial Pacific Ocean is markedly warmer, the ocean-atmosphere system is in a state called El Niño. Conversely, when the surface of the Equatorial Pacific Ocean is colder, the ocean-atmosphere system is in a state called La Niña. These states are extremely important for agriculture, population health, climate, weather, and many other sectors. Understanding what can lead to the ocean-atmosphere system shifting between El Niño and La Niña is vital. One variable that can impact the state of the system is vertical mixing. It can be determined by how water density and velocity changes with depth. In this study, three standard measures of mixing were compared. Data to calculate them was obtained with shipboard instruments during two research cruises: one in 2023 during a La Niña and one in 2024 during an El Niño. The ocean currents that flow at the equator were found to increase the potential for mixing during La Niña; El Niño was similar, though it was not found to have as strong mixing potentials. Though the region of EUC-induced shear did not show active mixing, this supports the evidence as it suggests that large-scale density inversions could not grow and were instead likely smoothed out quickly. These results were compared with those of three papers that used non-shipboard datasets and numerical models, generally agreeing. Comparing methods across location and time is important to understanding the broader impacts of ENSO on mixing and climate.

1. Introduction

ENSO is a naturally occurring ocean-atmosphere phenomenon that oscillates between El Niño and La Niña conditions, respectively defined as warm and cold anomalies in Eastern Equatorial Pacific SST. ENSO influences atmospheric conditions on a global scale. This atmospheric impact on the world is far-reaching. In the United States, El Niño is associated with increased hospitalizations due to vector-borne diseases (Fisman et al., 2016) and La Niña with increased damages due to hurricanes (Pielke & Landsea, 1999). Global sectors impacted by ENSO include agriculture, fishing, tourism, and population health and safety.

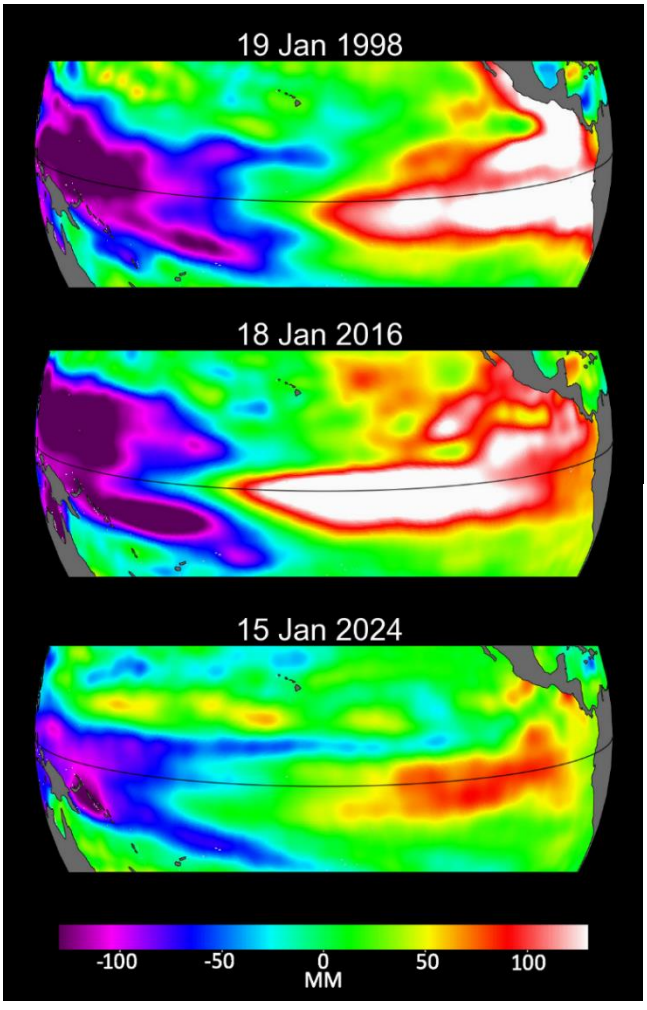

Figure 1. SSH anomaly in mm before the winter peak for two notably strong El Niños and the apparent peak of the 2023-2024 El Niño. Higher and lower SSH regions are shown by reds/whites and blues/purples, respectively. The thin black line indicates the Equator. Figure generated with NASA SSH satellite data. Figure from NASA, 2024.

El Niño and La Niña can be divided into warming and cooling stages, with both the beginning of an El Niño and the ending of a La Niña defined as warming (Deppenmeier et al., 2021). After three years of La Niña conditions, the equatorial Pacific experienced a major shift in SST and sea surface height (SSH) in 2023, marking the arrival of a warming El Niño winter in 2024.

Mitigation of negative ENSO impact can depend on predicting the temporal scale and magnitude of its oscillations. Continued study of the ocean and atmosphere conditions that control ENSO is crucial for this. Though El Niño forecast centers suggested 2023 could be notable in severity, comparative satellite SSH measurements demonstrate it was not as extreme as the El Niño events of 1997 or 2015 (Fig. 1).

The plethora of interconnected systems that control ENSO oscillations render it dynamic and non-trivial; however, components that impact it can be identified. ENSO can be influenced by positive feedback between SST and the trade winds. During a La Niña, the trade winds intensify, forcing surface water to build up in the Western Equatorial Pacific. The zonal pressure gradient due to SSH difference produces the EUC that flows eastward predominantly between 2^{o} S to 2^{o} N around 180° and 167° West, the longitudes of interest (Fig. 2). The shear between this and the oppositely directed surface current induces vertical mixing, and heat can be sequestered to depth (Deppenmeier et al., 2021). This can cool the surface, which intensifies the trade winds (Yang et al. 2022). Surface cooling is especially potent in the Eastern Equatorial Pacific, giving rise to a phenomenon known as the Equatorial Cold Tongue. It should be noted that this region is strongly controlled by upwelling, an equatorial feature distinct from vertical mixing.

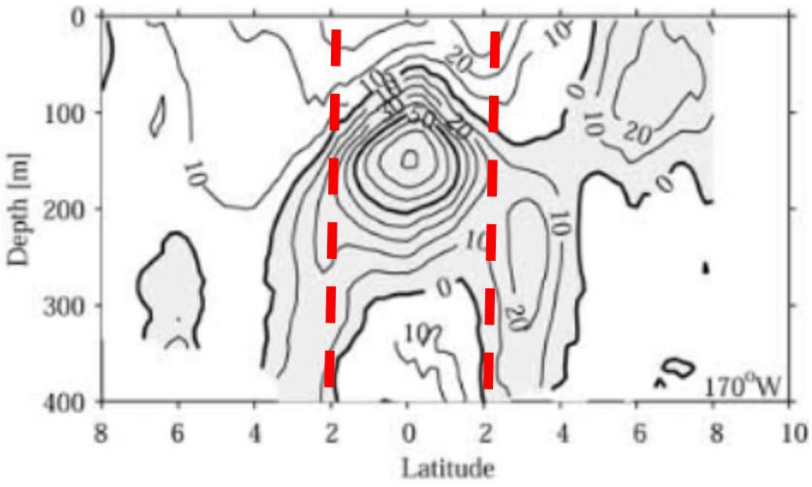

Figure 2. El Niño mean velocity with depth and latitude at 170° West. Contours indicate mean zonal velocity; the contour interval is 10 cm/s and heavy contours are at 50 cm/s intervals. Red dashed lines draw attention to the region between 2° S and 2° N. This figure was generated with averaged cruise data from the 1990's during El Niño conditions. Figure after Johnson et al. 2002, red dashed lines added.

During an El Niño, the trade winds weaken or reverse direction in the Eastern Equatorial Pacific, resulting in lower Western Equatorial Pacific SSH (FIG 1), a slower EUC, reduced mixing, and a warm SST that diminishes the trade winds further. The arrivals of both El Niño and La Niña can result in more extreme conditions with time. While satellites make atmospheric and surface-ocean conditions readily accessible, sub-surface phenomena are less documented. In the context of an equatorial heat budget, the most important impacts on SST are solar heating and vertical mixing (Deppenmeier et al., 2021). Therefore, quantifying how vertical mixing strength changes with ENSO conditions is important to understanding the broader system. This project employed three metrics to quantify turbulent, vertical mixing: Richardson numbers R_i (Eq. 1), Thorpe Scales L_T (Eq. 2), and turbulent dissipation rates ε (Eq. 3) from two meridional sections across the equator at the longitudes of interest.

A powerful method that can be employed to identify potential for mixing uses the relationship between intense turbulence and strong shear, i.e., changes in current velocity and direction with depth, as observed by an ADCP (Nystrom et al. 2007). There is an inherent competition between stratification and shear in the control of turbulence as indicated in their ratio, R_i. The greater the shear, the greater the turbulent mixing as internal waves on water layer interfaces are induced. The lesser the stratification, the greater the turbulent mixing as the water column becomes less stable. Thus, lower R_i denotes more mixing potential.

$$R_i = \frac{N^2}{S^2} \quad \text{(Eq. 1)}$$

The Richardson number R_i is described in Eq. 1 where shear $S = \frac{\partial u}{\partial z}$ (Galperin et al. 2007). $N = \sqrt{\frac{g}{\rho_0}\frac{\partial \rho}{\partial z}}$ is buoyancy frequency, a measure of the stratification with units Hz where ρ_0 is the density of seawater (Cusack et al. 2022) selected near the shear max. Mixing is significant and turbulent when the unitless numbers are below a critical value of 0.25 (Galperin et al. 2007).

$$L_T = \sqrt{\overline{d^2}} \quad \text{(Eq. 2)}$$

The Thorpe Scale method L_T is described in Eq. 2 where *d* is a water parcel's vertical displacement from buoyant equilibrium; it quantifies the density-driven vertical overturns in a depth profile by sorting it into a stable one measuring the vertical displacements of individual water parcels (Cusack et al. 2022, Gargett and Garner, 2008). This is a proxy for the overturn scale with the root mean square displacement (Cusack et al. 2022, Gargett and Garner, 2008). The Thorpe method is based on observing density instabilities within high resolution CTD profiles. Density inversions with depth are strong indicators of active mixing (Caulfield, 2021).

These density inversions are caused by breaking internal wave structures at the interface between two layers in the fluid, gradually mixing the two in turbulent spirals (Wykes and Dalziel, 2014). It should be noted that density in the Equatorial Pacific is predominantly controlled by temperature, not salinity. On prolonged time scales, density-driven mixing results in more homogeneous temperature with depth. If water is already well-mixed, then density-driven mixing will be reduced as there is less of a driving force to make internal waves break. A drawback to only considering density profiles is they could have been homogenized previously, regardless of the magnitude of potential mixing where they were measured. Furthermore, if the shear discussed in Eq. 1 is not strong enough, overturning may not happen at all. Regardless, high magnitude L_T layers are high in ε (Eq. 3) value, implying stronger internal wave energetics.

$$\varepsilon = C_0 \; L_T^2 \; N^3 \qquad \text{(Eq. 3)}$$

The turbulent diffusivity of kinetic energy ε measures the magnitude of vertical mixing (Cusack et al. 2019) and is shown in Eq. 3 where C_0 is an $O(1)$ proportionality constant and N is defined in Eq. 1. ε is elevated when more kinetic energy is spread out to be absorbed by the water due to greater turbulence and mixing (Woods, 1980). In the context of the Equatorial Pacific, ε acts against solar heating, cooling the sea surface.

Research on mixing in the Equatorial Pacific is ongoing; the consideration of three recent studies build context for the analysis of research cruise data. A study of a decade of monthly-averaged data from NOAA's Tropical Atmosphere Ocean (TAO) mooring in the Equatorial Cold Tongue at 0^o, 140^o West provide EUC depth, TIW forcings, and resultant ε between warming and cooling El Niños and La Niñas (Fig. 3, Warner & Moum, 2019). EUC depth is greater in warming El Niños than warming La Niñas, and TIW forcings are stronger during warming La

Niñas, supporting the greater mixing values (Fig. 3). TIWs are a collection of equatorial wave phenomena (Moum et al. 2009) that increase mixing beyond the 'background state.' The data from χpods, instrumentation that measures the fine-scale temperature structures that lead to inferences on turbulence, demonstrate that ε and thus mixing is most diminished during warming El Niños and much stronger during warming La Niñas (Fig. 3).

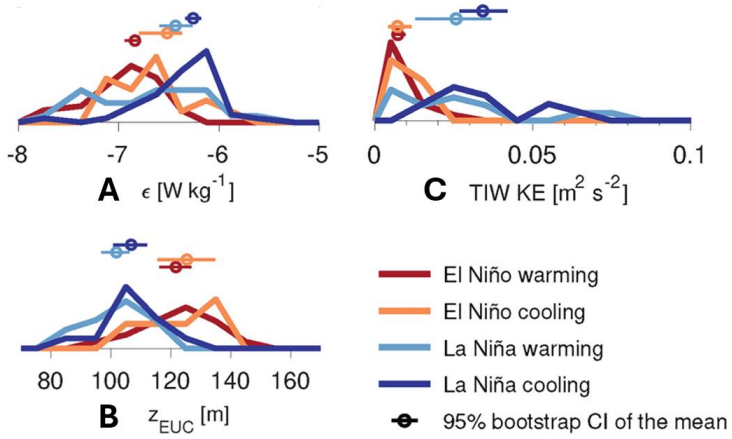

Figure 3. (A) ε from χpods between 29 and 69 m. (B) EUC core depth. (C) Tropical instability wave kinetic energy. Each histogram is composed of four sub-histograms denoting the ENSO regimes from monthly [0°, 140° West TAO mooring] averages. Means are shown as circles, the 95% bootstrap confidence intervals of the means are lines. Figure and caption from Warner & Moum, 2019.

ARGO floats drift with the ocean's currents, descending to sample such variables as temperature, salinity, and pressure before surfacing to report data. These drifter's data were analyzed for instances of L_T events across the equator both latitudinally and longitudinally (Liu et al., 2016). Over the 14 years of data, many of these events were identified at and around the longitudes of interest, centered between 2° S and 2° N (Liu et al., 2016). These mixing events were the results of the shear from TIWs and between the EUC and surface currents above the EUC max (Liu et al., 2016, Fig 4). TIWs potentially instigated some of these events as mixing

was found to be higher during both La Niñas and times of TIW presence (Liu et al., 2016).

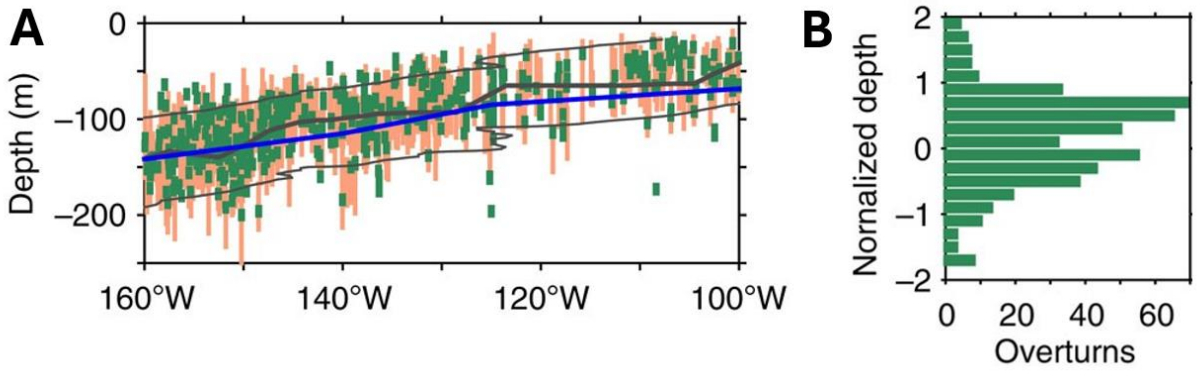

Figure 4. (A) Depth and overturn scale (m) of events between 3° S and 6° N in green, instantaneous pycnocline layers in orange, EUC center is a blue line, the center and bounds of the mean pycnocline are thick black curves and thin black curves. (B) Histogram of overturn events. Figure and caption after Liu et al., 2016.

While study of data from cruises, satellites, floats, and moorings is crucial, development of models to simulate environmental conditions is also important for cost-effective analysis of large climate systems. A study of mixing in the Equatorial Pacific Cold Tongue at 0 °, 140° West with model data from the Parallel Ocean Program (POP2) found El Niño to exhibit lesser S^2 and thus lower R_i (Eq. 1) values than during a La Niña (Fig. 5, Deppenmeir et al. 2021).

The lowest R_i values for both El Niño and La Niña were found in the upper 100 m of water (Fig. 5), corresponding to where shear from the EUC is likely strongest (Fig. 2); it should be noted, though, that mixing is often elevated in the upper water column due to surface interactions. The EUC is also shown in the zonal component of velocity (Fig. 5). Considering much research focuses on mixing in the Eastern Equatorial Pacific, studying mixing near the center longitudes is important to characterizing ENSO-controlled vertical mixing zonally across

the Equator. In this study comparing ADCP and CTD data from two cruises, one during an El Niño and the other during a La Niña, these central longitudes are explored.

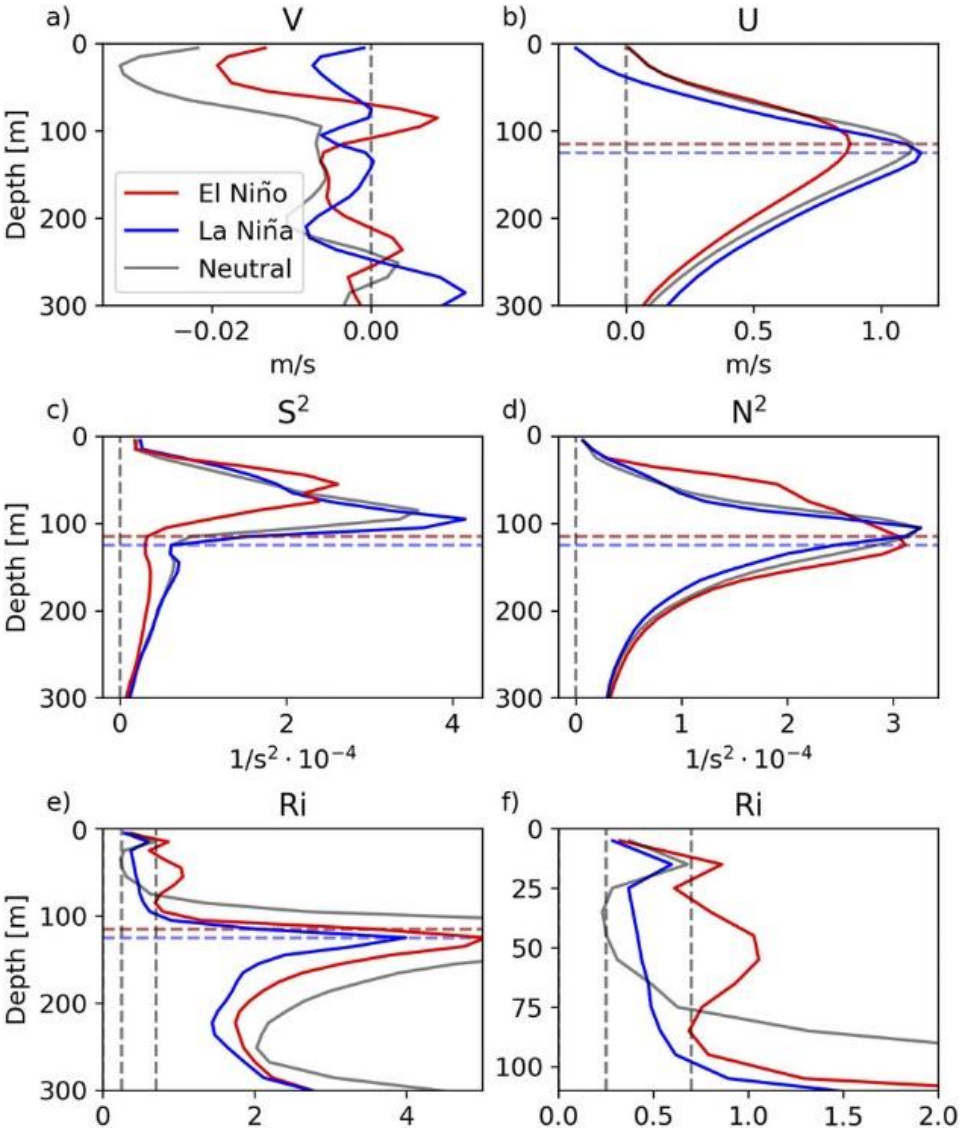

Figure 5. POP2 profiles at 0°, 140°W for El Niño (red), La Niña (blue), and neutral (black) conditions: (a) meridional and (b) zonal velocity components and (c) total shear squared and (d) buoyancy squared, from which (e) the gradient number R_i is calculated. Dashed horizontal lines show the depth of the EUC maximum per ENSO condition (Deppenmeier et al. 2021). (f) shows zoomed-in R_i for the upper 100 m of the water column. Figure and caption after Deppenmeir et al. 2021.

It was hypothesized that vertical mixing during a warming El Niño would be decreased compared to a warming La Niña and it was expected that these results would be consistent with those from TAO mooring array, ARGO float, and POP2 model data. The results from these datasets are a result of the slowed EUC and diminished shear during the warming El Niño.

2. Methods

While moorings and floats can provide a wealth of data at specific or roving locations across time (Fig. 3), ship-based measurements can be useful for directly measuring the ocean state along a high-resolution transect. Data from the TN 413 cruise on the R/V Thomas G. Thompson out of Honolulu in late February 2023 across the Equator along 180^{o} were used in the equations described above to determine La Niña mixing metrics (Fig. 6). El Niño mixing metrics were calculated in the same way with data from the TN 427 cruise on the R/V Thomas G. Thompson out of Pago Pago, American Samoa between 28 December 2023 and 11 January 2024 along 167^{o} W (Fig. 6). Both cruises' data were taken, processed, and cleaned with the methods described below.

For both cruises, the main cross-Equator sampling route was from 5^{o} S to 5^{o} N with casts using a SeaBird 9+ CTD occurring every degree of latitude (Fig. 6). In the 2023 cruise between 2^{o} S and 2^{o} N, the SeaBird 9+ CTD sampled every half degree of latitude. In the 2024 cruise between 1^{o} S and 1^{o} N, the SeaBird 9+ CTD sampled every half degree of latitude. These CTD casts provided temperature and salinity, and temperature was predominant in characterizing water column stability. The CTD data was post-processed using standard Sea-Bird CTD processing software following the GO-SHIP protocol (McTaggart et al., 2010). The data from

each downcast was isolated and pressure values that were not monotonically increasing were eliminated.

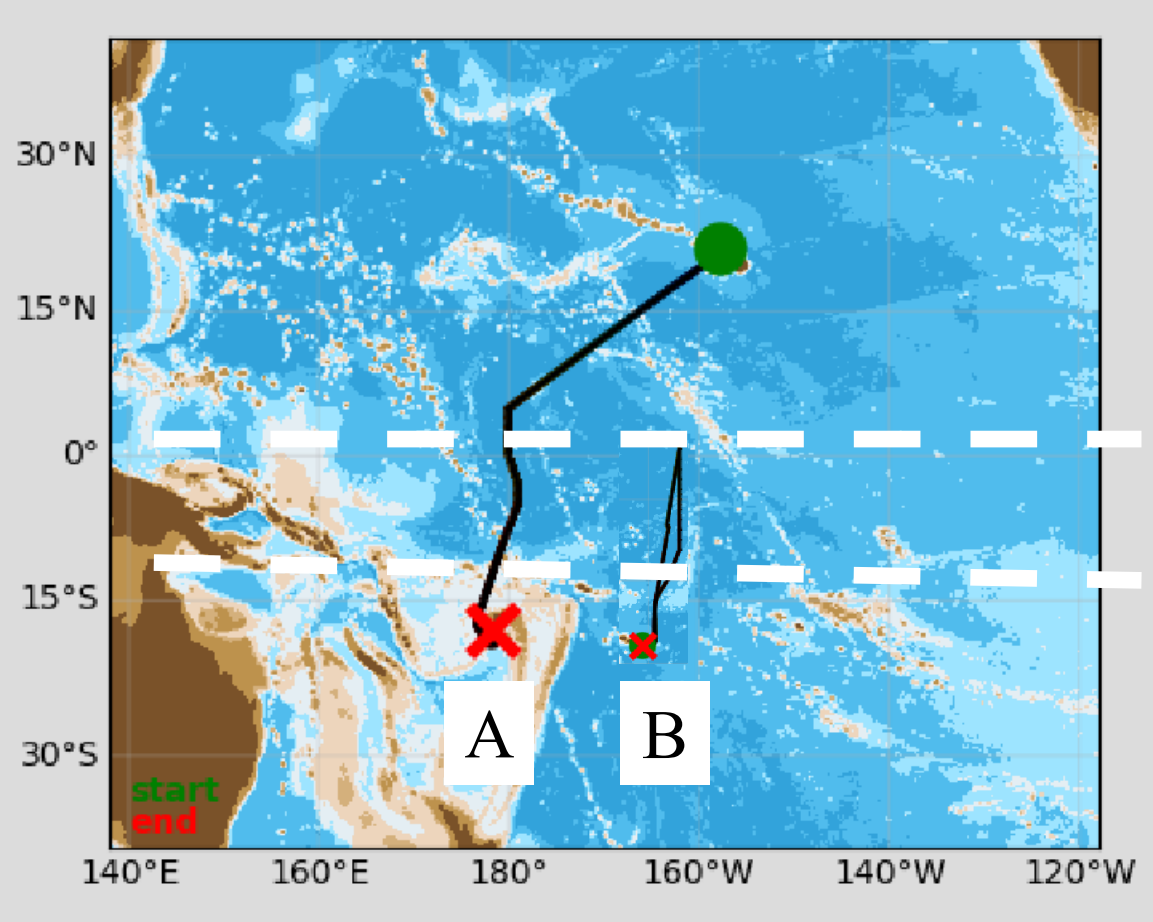

Figure 6. (A) La Niña Cruise TN 413 2023. (B) El Niño Cruise TN 427 2024. Black lines indicate the cruise paths. White dashed lines indicate 5° S and 5° N. The large green circle shows Honolulu, Hawaii, the start port for cruise (A). The large red 'x' symbol shows Suva, Fiji, the end port for cruise (A). The smaller red 'x' symbol shows Pago Pago, American Samoa, the start and end port for cruise (B). Figure constructed from UHDAS+CODAS dataviewer.py function.

The ship's 75kHz OS75nb ADCP operated continuously during both TN 413 and TN 427 cruise. For the El Niño 2024 cruise, ADCP data from the first crossing of the equator (Fig. 6) was primarily used as the two crossings were relatively similar with regards to resultant R_i when calculated with the same CTD data. Mounted to the vessel's hull, the ADCP was used to measure zonal water velocities, averaged over discrete depth bins. ADCP data was post-processed using

UHDAS+CODAS software from the University of Hawaii available at https://currents.soest.hawaii.edu/docs/adcp_doc/index.html (accessed on 12/28/2023, Firing et al. 2012).

Threshold editing was applied to both cruises' data to eliminate velocity values in bin ensembles with less than 80% good pings or greater than 500 mm/s error velocity magnitude. For both cruises, in addition to removing all data beyond 5° S and 5° N to obtain a transect, data from depths greater than 650 m were removed as many values in deeper depths were flagged during threshold editing. For the TN 413 cruise, a final phase correction of 0.21 radians and a final amplitude correction of 1.012 was applied, resulting in median water-track calibration bias estimates of 0.9970 for amplitude and 0.0070° for phase. For the TN 427 cruise, phase correction was not warranted, but a final amplitude correction of 1.006 was applied, resulting in median water-track calibration bias estimates of 1.0005 for amplitude and 0.0525° for phase.

Mixing metrics were evaluated through 300 m for both cruises as the velocity of the EUC was greatest at around 170 m of depth near 167° W and 150 m of depth near 180 ° (Johnson et al. 2002). Neglecting vertical and meridional velocity relative to the much larger zonal velocity components, shear, $\frac{\partial u}{\partial z}$, was calculated from the velocity profiles by taking the gradient of velocity with respect to depth using the *numpy gradient* function (accessed on 12/28/23, https://numpy.org/doc/stable/reference/generated/numpy.gradient.html). The approximate depth of greatest shear was determined, and median shear values in the spatial box defined between 2° S and 2° N, and 75 m and the EUC depth were found. This spatial box cut mixing in the surface and at depth, focusing latitudinally on the impact of EUC-induced shear. N^2 as a function of latitude was found by calculating accordingly (Eq. 3) and interpolating between each CTD cast linearly. Using the calculated shear and N^2, R_i (Eq. 1) was determined with depth and latitude. R_i

distributions in the spatial box were found. R_i probability density functions (PDF) were found by normalizing these R_i distributions.

Metrics for diapycnal mixing intensity (Eq. 2) were calculated from the CTD profiles with the use of python package *mixsea* (Cusack et al. 2022) and its dependencies with *matplotlib* used for data visualization (accessed on 12/28/23, https://matplotlib.org/). *Mixsea's* overturn.eps_overturn function was used to return L_T (Eq. 2) for the mixing layers at each CTD cast location (Cusack et al. 2022).

To calculate the ε (Eq. 3) with L_T, missing values were removed. *Mixsea's* overturn.eps_overturn function was again used to evaluate each identified mixing layer's ε (Cusack et al. 2022) value based on an overturn ratio criterion of 0.2 to reject patches of asymmetry that likely came from instrumental error (Cusack et al. 2019).

With the data from 2024's warming El Niño and 2023's warming La Niña cruises, the mixing metrics were calculated following the above descriptions. The results were qualitatively compared with the results of Warner & Moum, 2019 (Fig. 3), Liu et al., 2016 (Fig. 4), and Deppenmeier et al. 2021 (Fig. 5). In the event of sampling over a TIW, mixing values would have been elevated (Moum et al. 2009). However, there was no evidence either cruise occurred during the presence of TIWs as determined with NASA's SOTO: https://soto.podaac.earthdatacloud.nasa.gov/.

3. Results

Mixing can be driven between strong, oppositely directed currents within regions of weak stratification. Considering these metrics and their spatial distributions was important to understanding the mixing parameters R_i, L_T, and ε.

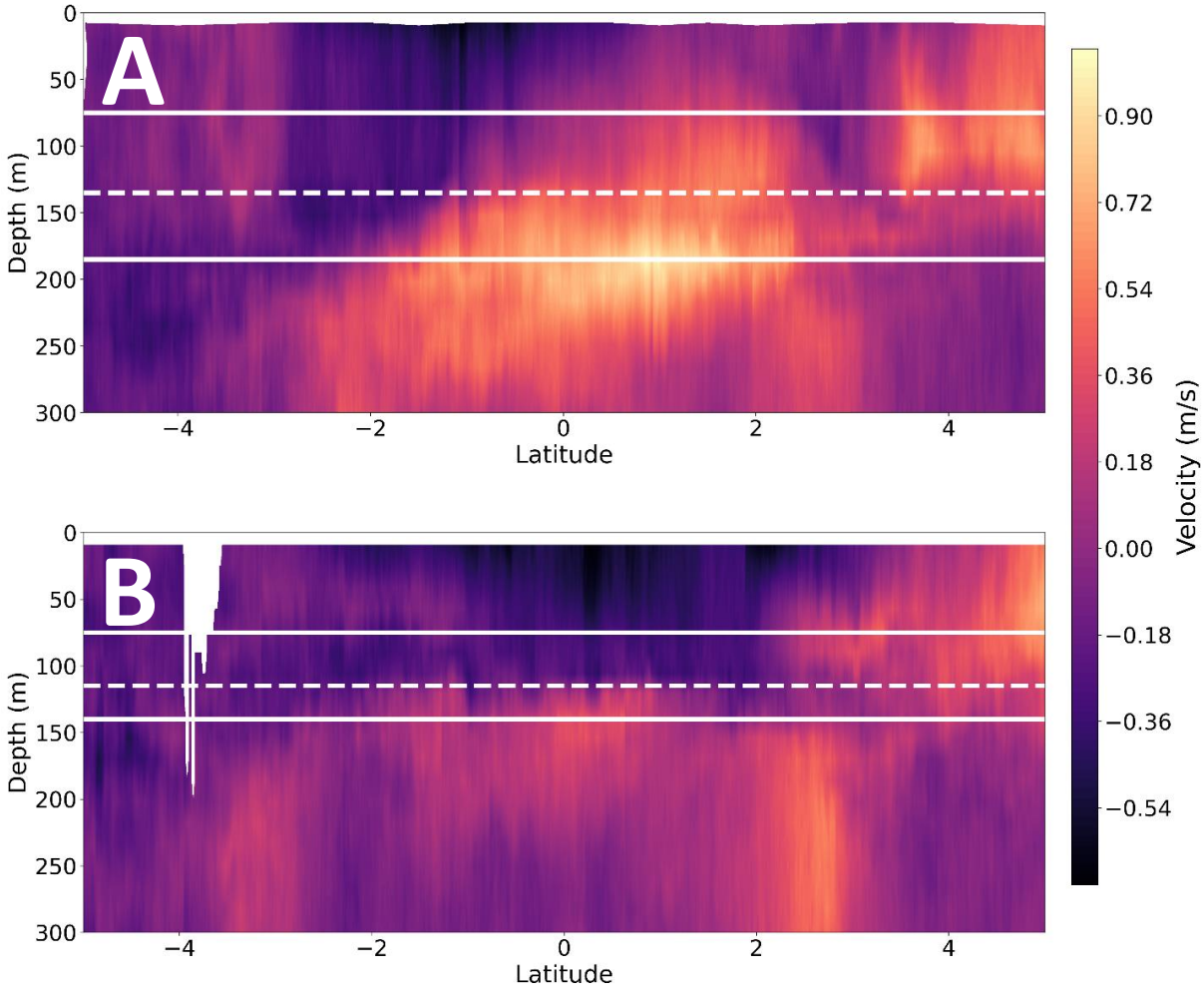

Figure 7. Zonal velocity. Sign denotes direction with positive being westward. (A) 2023, 180°. (B) 2024, 167° West. The horizontal dashed white lines indicate the depth of greatest shear at the equator. The upper solid white lines indicate 75 m, and the bottom solid white lines indicate the center of the EUC as estimated from velocity data. The white at around -4° in (B) is a patch of bad data removed during ADCP post-processing.

The 2023 surface current was slightly weaker than the 2024 surface current, which was also broader, spanning between 2° S and 2° N (Fig. 7). In contrast to the surface current, the velocity of the EUC during 2023 was stronger than that of 2024 by roughly a factor of two (Fig. 7). Similarly to the EUC's center, the depth of greatest shear was deeper in 2023 at 135 m than in 2024 at 115 m (Fig. 7). As a result of the EUC and surface current velocities, the shear in 2023

was stronger than in 2024 and shifted South of the equator. In the spatial box focused on EUC-induced mixing, the median shear in 2023 was 0.0084 Hz, while the median shear in 2024 was 0.0058 Hz.

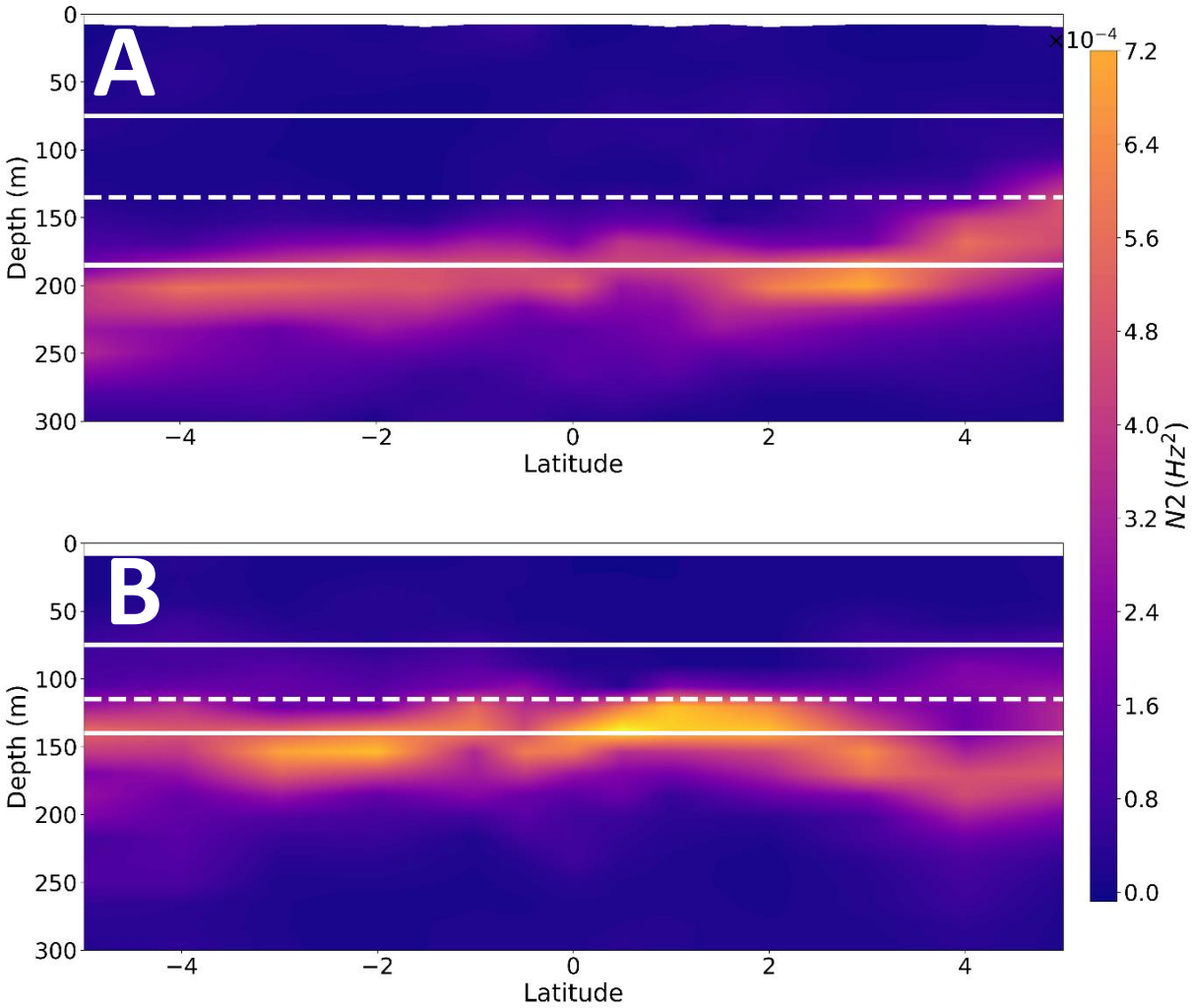

Figure 8. Buoyancy Frequency. (A) 2023, 180°. (B) 2024, 167° West. The horizontal dashed white lines indicate the depth of greatest shear at the equator. The upper solid white lines indicate 75 m, and the bottom solid white lines indicate the center of the EUC as estimated from velocity data.

Corresponding to the depth of the thermocline, a distinct band of relatively elevated N^2 spanned both transects (Fig. 8). These bands were at the depth of the EUC centers, 185 m in 2023 and 140 m in 2024 (Fig. 8). In 2023, the shear max at the equator was far enough from the

EUC center that it was almost completely out of the band of high stability (Fig. 8). In 2024, the shear max at the equator was within the band of high stability (Fig. 8).

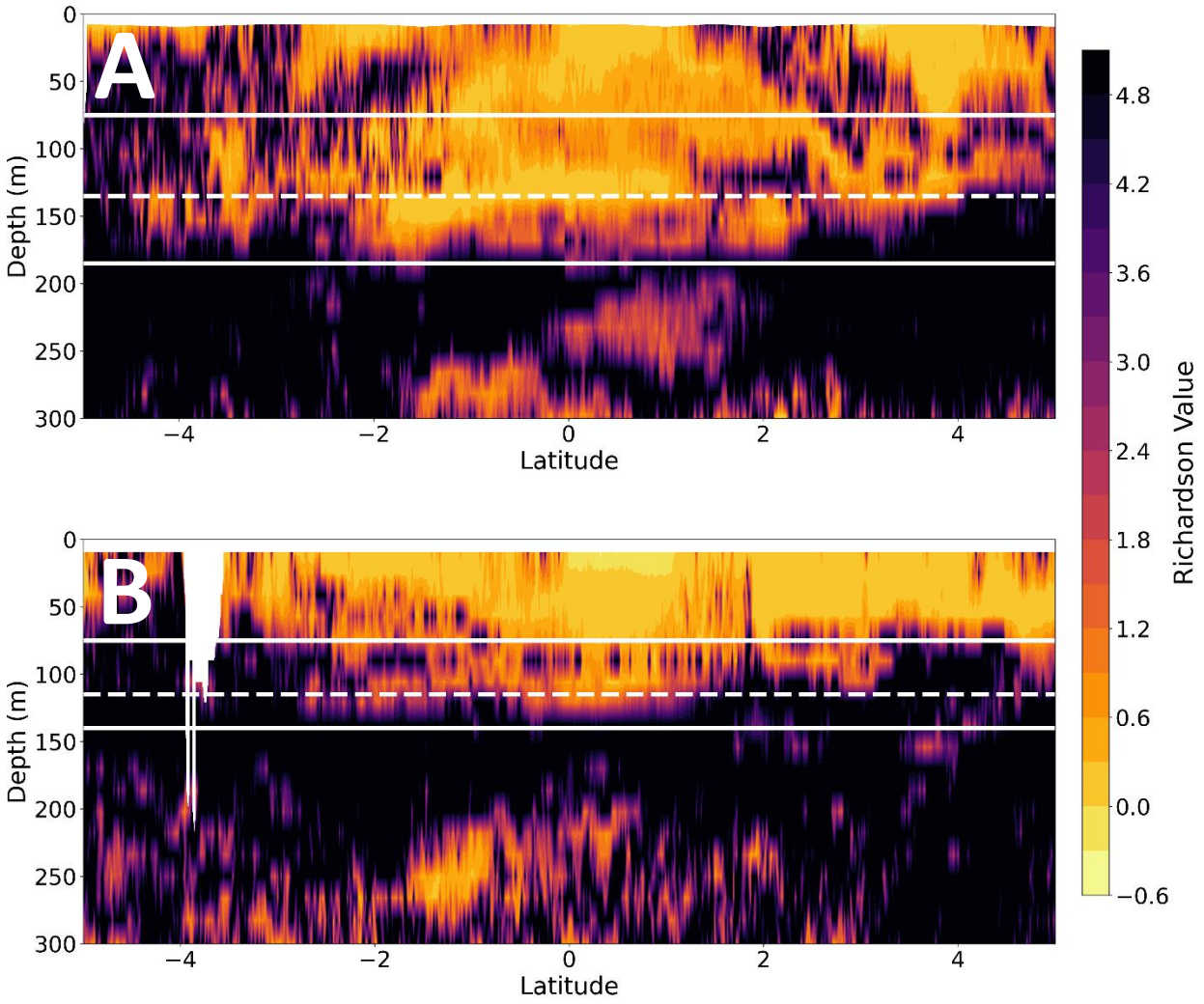

Figure 9. Spatial Distribution of Richardson Numbers. (A) 2023, 180°. (B) 2024, 167° West. The horizontal dashed white lines indicate the depth of greatest shear at the equator. The upper solid white lines indicate 75 m, and the bottom solid white lines indicate the center of the EUC as estimated from velocity data. The white at around -4° in (B) is a patch of bad data removed during ADCP post-processing.

The spatial distribution of significant R_i (R_i < 0.25) differed between 2023 and 2024 in depth, and structure. (Fig. 9). As the upper layers of significant R_i extended to just above the EUC centers in both years, the 2023 layer reached deeper than the 2024 layer (Fig. 9). This

resulted in the thickness of the layer of significant R_i during 2023 exceeding that determined in 2024 by 45 m (Fig. 9). While the 2023 significant R_i top layer was centered between 2° S and 2° N, the 2024 significant R_i top layer was more spread out (Fig. 9).

This is evident with the consideration of the structure, or patchiness, of the significant R_i upper layers. While the 2023 significant R_i top layer was broken up by fragments of R_i greater than 0.25 within the region between 2° S and 2° N, the 2024 significant R_i top layer was relatively uniform in the upper 75m, while chunks of R_i less than 0.25 fragmented the lower sections of the layer throughout the transect (Fig. 9). Of greatest importance, the 2023 significant R_i top layer between 2° S and 2° N exhibited lesser magnitudes of R_i compared with the slightly greater R_i in 2024 at the same depths (Fig. 9). The smallest magnitudes of R_i in 2023 occurred between 2° S and 2° N at a depth equal to the shear max; at the same depth in 2024, R_i were greater and fragmented (Fig. 9).

Another way to consider the distributions of R_i between the two years was to compare the PDFs of R_i in the spatial box focused on EUC-induced mixing. There were less R_i between 1 and 10 in 2023 than in 2024 as the integrated probability density of normalized R_i in this range was 0.43 for La Niña 2023 and 0.63 for El Niño 2024 (Fig. 10). Conversely, there were more significant R_i in 2023 than in 2024 as the integrated probability density of normalized R_i distributions between 0 and 0.25 R_i was 0.33 for La Niña 2023 and 0.17 for El Niño 2024 (Fig. 10).

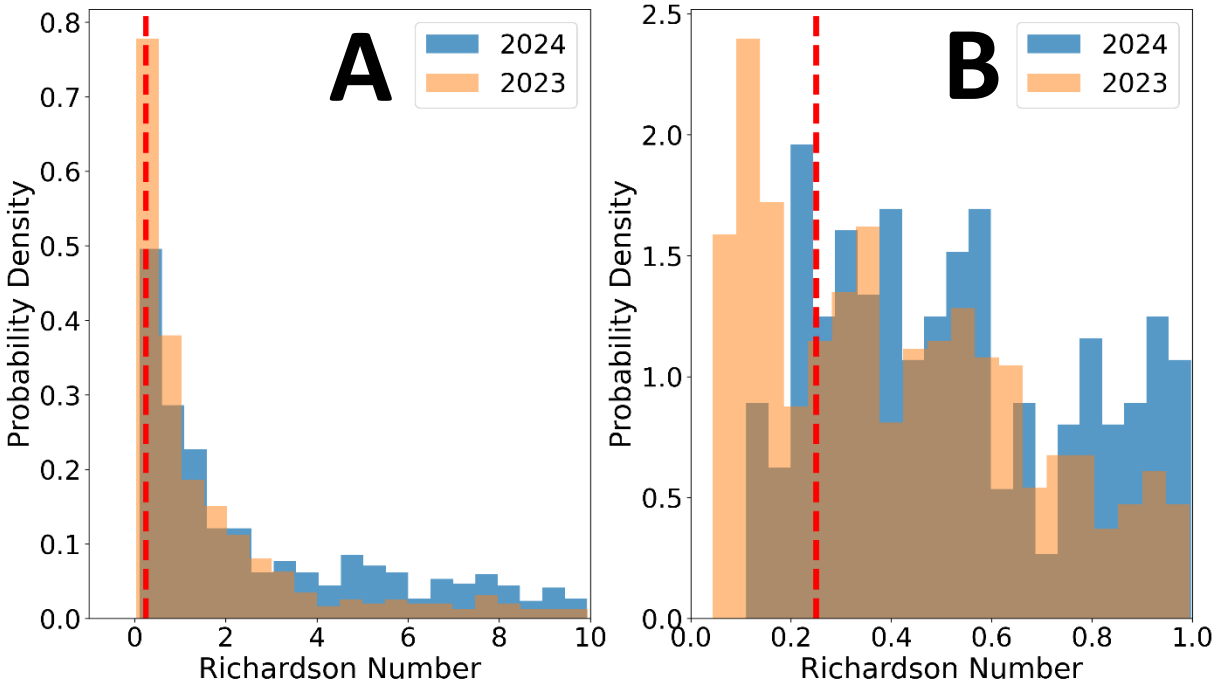

Figure 10. PDF distribution of Richardson Numbers normalized by count. Panel A: Full Distribution. Panel B: Significant Richardson Number Range. The red dashed lines show Ri= 0.25. Data comes from the regions of elevated mixing potential, i.e., between 2o S and 2o N and between 75m and the EUC depth, corresponding to between the solid white lines in FIG. 8, 9, 10, and 12.

Both years had the largest L_T and ε values near the surface with another strong layer deeper than the EUC center (Fig. 11). The depth ranges between both years' surface and deep mixing layers roughly align with the lower extents of the significant R_i upper layers between 2° S and 2° N. The distributions of ε values were similar in both years (Fig. 11). Most ε values were around the magnitude of $1*10^{-6}$ (Fig. 11). 2023 only had one L_T event in the regions of elevated mixing potential, while 2024 had three smaller-scale events (Fig. 11). All four events were outside the latitude range to be associated with EUC-induced shear (Fig. 11).

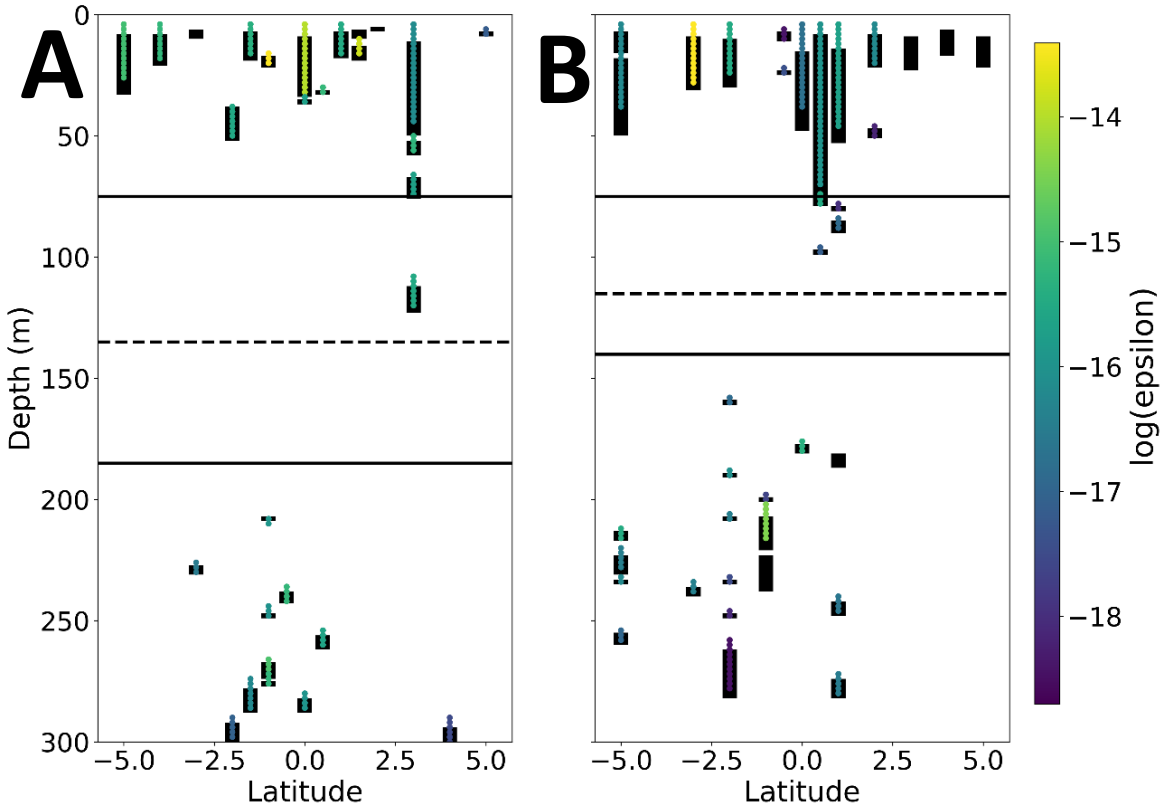

Figure 11. L_T and ε. (A) 2023, 180°. (B) 2024, 167° West. Black bars show location and vertical scale of L_T. Dots show location of significant ε values, with color denoting the log of the magnitude. Note that 10 to the power of the minimum ε, -18.7, is $1.995*10^{-19}$ and 10 to the power of the maximum ε, -13.4, is $1.5 * 10^{-6}$. The horizontal dashed black lines indicate the depth of greatest shear at the equator. The upper solid black lines indicate 75 m, and the bottom solid black lines indicate the center of the EUC as estimated from velocity data.

4. Discussion

Results were consistent with the hypothesis: the magnitudes of mixing metrics were greater during the 2023 La Niña than in the 2024 El Niño. Although both years had regions of elevated mixing potential due to EUC-surface interactions, these mixing metrics were greater in magnitude and structure in 2023. Zonal currents were greater and more focused in 2023 than 2024 (Fig. 7), resulting in greater magnitudes of shear in 2023. This could be a direct result of increased EUC due to La Niña. Potentially a result of prior mixing from La Niña conditions, the

thermoclines and resulting bands of strong N^2 were deeper in 2023 than in 2024 (Fig. 8). This resulted in a greater area and structure of significant R_i due to EUC shear in 2023 than in 2024 (Fig. 9). R_i results in 2024 were likely due to reduced shear from the EUC combined with the stronger, shallower N^2 band. Because 2024 exhibited larger values of R_i in the minimum contour (Fig. 9), there was less potential for mixing. In the spatial box between 75 m and the EUC and 2° S and 2° N, greater integrated probability densities of significant R_i in 2023 supported stronger mixing potential due to La Niña increased shear (Fig. 10). L_T and elevated ε events in the surface were likely due to surface mixing; at depth, they were likely due to the shear between the EUC and deeper currents. In both years, L_T and elevated ε events were almost completely absent from the spatial box of elevated mixing potential described above (Fig. 11). However, the lack of a substantial number of these events does not necessarily constitute a lack of mixing. As these two metrics are event-based and actively stabilize water columns, it is possible that overturns were small-scale due to constant mixing occurring here because of the environmental forcings (shear and N^2). Especially in 2023, the water was likely well-mixed, as evidenced by the significant R_i distributions (Fig. 9).

It is important to consider the environmental context that influenced these metrics. Differences in time and location between the two cruises make it necessary to consider how mixing metrics might be inherently dissimilar when comparing the two. The EUC shoals towards the east and is depth-modulated by ENSO, with deeper current cores found during El Niño (Fig. 3). This impacted the magnitudes of mixing relative to depth given the difference in longitude. While the 2023 cruise was at 180°, the 2024 cruise was at 167° West. Due to eastward EUC shoaling (Fig. 4), the 2024 EUC's shallower thermocline and N^2 band were in part caused by the difference in cruise longitude. However, it should be noted that the difference in EUC depth

between the two cruises was greater by around 10 m than what would be expected from the impact of shoaling (Johnson et al. 2002). The 2023 cruise was in late February of a warming La Niña; the 2024 cruise was in early January of the peak of a warming El Niño. While the difference in time of year is likely not consequential, it is obvious that the difference in ENSO state was greatly impactful. As both cruises were during winter, mixing was likely elevated compared to other seasons (Deppenmeier et al. 2022). There was no evidence of TIWs in satellite products. As more mixing can occur during the presence of TIWs (Moum et al. 2009), this project's results can be considered as demonstrating the 'background state' of the ocean.

Comparing these results with previous studies utilizing different sampling methods is important to validate the quality of the various methods. A study of the distributions and averages of mixing forcings and parameters from TAO data considered the impacts of TIWs (Warner & Moum, 2019); how these results compare with cruise data from periods without TIWs demonstrates how TIWs elevate mixing from the 'background state.' Comparison of the study's La Niña warming and El Niño peak warming with the 2023 and 2024 cruises, respectively, reveal similar EUC depth trends, that is, La Niña warming EUC depths were deeper than El Niño peak warming EUC depths (Fig. 3; Fig. 7). This supported similar mixing results: ε distributions from TAO data (Fig. 3) were similar in magnitude to ε values calculated from cruise data with *mixsea* (Fig. 11). Especially with regards to the forcings, these qualitative similarities support the validity of one another. Furthermore, the slightly elevated ε values from TAO data demonstrate how factoring in TIW energy increases overall mixing metrics (Warner & Moum, 2019).

The results of a study that used both TAO and ARGO data to map L_T over a range of years by latitude and depth (Liu et al., 2016) established how limited L_T events are at the depths of

interest. Despite the years of data the study incorporates, there were no more than a couple hundred events reported (Fig. 4). It was not surprising, then, that data from cruises on the timescale of two weeks did not show many of these events occurring at the depths of interest (Fig. 11). It was likely that large-scale L_T events greater than a couple meters were rare because the environmental forcings induced small-scale L_T events to quickly remix the system before large density inversions grew. L_T events on the scale of tens of centimeters to a couple meters were averaged out by both the ARGO float bin sizes (Liu et al., 2016) and the 2023 and 2024 cruise processed CTD bin sizes.

POP2 numerical model results at 140° West indicated similar qualitative trends between El Niño and La Niña mixing as this study's cruise results (Deppenmeir et al. 2021); however, comparison suggested the POP2 model may have overestimated the difference between La Niña and El Niño R_i. As the POP2 study was further East, the EUC was shallower, leading to shallower EUC velocity and shear maximums, N^2 bands, and significant R_i layer depths than the 2023 and 2024 cruises (Fig. 5, 8, 9, 10). Though mixing increased in range and magnitude to the East (Deppenmeir et al. 2021), overall POP2 R_i were larger in magnitude than cruise results by a factor of roughly two, (Fig. 5 and 10) potentially due to the model inputs of POP2 (Deppenmeir et al. 2021). The POP2 model suggested that La Niña R_i would on average be lower than El Niño R_i by a factor of 1.5 at around 80 m of depth (Fig. 5); conversely, cruise results indicated that the difference may be less extreme (Fig. 9 and 11). This could indicate that the POP2 model overestimated the difference in mixing magnitudes between El Niño and La Niña.

5. Conclusion

It was expected there would be greater mixing signals in the La Niña 2023 cruise compared with the El Niño 2024 cruise. This was confirmed with the R_i distributions; there were greater potentials for mixing during the La Niña and a lack of L_T events close to the shear max suggested the system's quick smoothing of density inversions. These findings support previous literature utilizing various methods and models: TAO (Warner & Moum, 2019), ARGO float and TAO (Liu et al., 2016), and POP2 model outputs (Deppenmeir et al., 2021). The subtle differences among these studies suggest variability with time, latitude, longitude, and environmental conditions such as the presence of TIWs. It also indicates the POP2 model may slightly overestimate the difference between La Niña and El Niño. The 'background state' of mixing determined in this study sets an important baseline for research incorporating TIWs. Further work could benefit from smaller depth bin sizes to tease out small-scale L_T events. There is also a current lack of direct quantitative comparison between the methods as exact mixing parameters and location vary significantly; a study attempting to directly reproduce results would allow for more quantitative comparison.

6. Acknowledgements

This work would not have been possible without the support and encouragement of my mentors and peers. I am incredibly thankful to Mark Warner for processing the CTD data, providing ideas, resources, and writing assistance. I thank Georgy Manucharyan for his provision of relevant papers and general explanation of TIWs and equatorial mixing. I would like to thank Susan Hautala for her encouragement and ADCP post-processing advice. On that subject, I am thankful for Julia Hummon helping me navigate the ADCP post-processing software. I am thankful for the other instructors of the OCEAN thesis classes for their lectures and help at sea

and on shore, Ginger Armbrust, Rick Keil, Kathy Newell, Andrea Ogston, and Francois Ribalet. I would like to thank my peers Yanfeng Shao and Kayla Robertson for their help with coding, and Alex Roberts and Sophie Jenness for paper editing. I greatly appreciate all my peers who were on the cruise running CTDs and other equipment; the team culture was incredible. I would like to thank the student researchers and crew of the R/V Thomas G. Thompson on expedition TN 413. I would like to thank the Washington NASA Space Grant Consortium for providing me with scholarship funding to attend the University of Washington and participate in wonderful experiences such as this. Finally, to the captain Erick Haroldson and crew of the R/V Thomas G. Thompson on expedition TN 427, I extend thanks for working with us, teaching us, and facilitating our scientific learning and growth.

References

Caulfield, C. P. (2021), Layering, instabilities, and mixing in turbulent stratified flows, *Annual Review of Fluid Mechanics*, *53*(1), 113–145, doi:10.1146/annurev-fluid-042320-100458.

Cusack, J. M., G. Voet, M. H. Alford, J. B. Girton, G. S. Carter, L. J. Pratt, K. A. Pearson-Potts, and S. Tan (2019), Persistent turbulence in the Samoan passage, *Journal of Physical Oceanography*, *49*(12), 3179–3197, doi:10.1175/jpo-d-19-0116.1.

Cusack, J., H. Drake, and G. Voet (2022), Mixsea 0.1.1 Documentation, *mixsea*. Available from: https://mixsea.readthedocs.io/en/v0.1.1/index.html (Accessed 29 November 2023)

Davies Wykes, M. S., and S. B. Dalziel (2014), Efficient mixing in Stratified flows: Experimental study of a rayleigh–taylor unstable interface within an otherwise stable stratification, *Journal of Fluid Mechanics*, *756*, 1027–1057, doi:10.1017/jfm.2014.308.

Deppenmeier, A.-L., F. O. Bryan, W. S. Kessler, and L. Thompson (2021), Modulation of cross-isothermal velocities with ENSO in the tropical pacific cold tongue, *Journal of Physical Oceanography*, *51*(5), 1559–1574, doi:10.1175/jpo-d-20-0217.1.

Deppenmeier, A.-L., F. O. Bryan, W. S. Kessler, and L. Thompson (2022), Diabatic upwelling in the tropical pacific: Seasonal and subseasonal variability, *Journal of Physical Oceanography*, *52*(11), 2657–2668, doi:10.1175/jpo-d-21-0316.1.

Firing, E., J. Hummon, and T. Chereskin (2012), Improving the quality and accessibility of current profile measurements in the Southern Ocean, *Oceanography*, *25*(3), 164–165, doi:10.5670/oceanog.2012.91.

Fisman, D. N., A. R. Tuite, and K. A. Brown (2016), Impact of el niño southern oscillation on infectious disease hospitalization risk in the United States, *Proceedings of the National Academy of Sciences*, *113*(51), 14589–14594, doi:10.1073/pnas.1604980113.

Galperin, B., S. Sukoriansky, and P. S. Anderson (2007), On the critical Richardson number in stably stratified turbulence, *Atmospheric Science Letters*, *8*(3), 65–69, doi:10.1002/asl.153.

Gargett, A., and T. Garner (2008), Determining Thorpe Scales from ship-lowered CTD density profiles, *Journal of Atmospheric and Oceanic Technology*, *25*(9), 1657–1670, doi:10.1175/2008jtecho541.1.

Johnson, G. C., B. M. Sloyan, W. S. Kessler, and K. E. McTaggart (2002), Direct measurements of upper ocean currents and water properties across the tropical Pacific during the 1990s, *Progress in Oceanography*, *52*(1), 31–61, doi:10.1016/s0079-6611(02)00021-6.

Liu, C., A. Köhl, Z. Liu, F. Wang, and D. Stammer (2016), Deep-reaching thermocline mixing in the equatorial Pacific Cold tongue, *Nature Communications*, *7*(1), doi:10.1038/ncomms11576.

McTaggart, K & Johnson, Gregory & Johnson, M & Delahoyde, F & Swift, J. (2010). Notes on CTD/O2 data acquisition and processing using Sea-Bird hardware and software (as available). GO-SHIP repeat hydrography manual: A collection of expert reports and guidelines.

Moum, J. N., R.-C. Lien, A. Perlin, J. D. Nash, M. C. Gregg, and P. J. Wiles (2009), Sea surface cooling at the equator by subsurface mixing in tropical instability waves, *Nature Geoscience*, *2*(11), 761–765, doi:10.1038/ngeo657.

NASA. 2024. El Niño 2023. JPL NASA. Available from: https://sealevel.jpl.nasa.gov/data/el-nino-la-nina-watch-and-pdo/el-nino-2023/ (Accessed 25 January 2024)

Nystrom, E. A., C. R. Rehmann, and K. A. Oberg (2007), Evaluation of mean velocity and turbulence measurements with ADCPs, *Journal of Hydraulic Engineering*, *133*(12), 1310–1318, doi:10.1061/(asce)0733-9429(2007)133:12(1310).

Pielke, R. A., and C. N. Landsea (1999), La Niña, El Niño and Atlantic hurricane damages in the United States, *Bulletin of the American Meteorological Society*, *80*(10), 2027–2033, doi:10.1175/1520-0477(1999)080<2027:lnaeno>2.0.co;2.

Warner, S. J., and J. N. Moum (2019), Feedback of mixing to ENSO phase change, *Geophysical Research Letters*, *46*(23), 13920–13927, doi:10.1029/2019gl085415.

Woods, J. D. (1980), Do waves limit turbulent diffusion in the ocean?, *Nature*, *288*(5788), 219–224, doi:10.1038/288219a0.

Yang, F., L. Zhang, and M. Long (2022), Intensification of pacific trade wind and related changes in the relationship between sea surface temperature and sea level pressure, *Geophysical Research Letters*, *49*(8), doi:10.1029/2022gl098052.